Supporting Information

Hydrogen spillover enabled active Cu sites for methanol synthesis from CO_2 hydrogenation over Pd doped CuZn catalysts

Bing Hu[a], Yazhi Yin[a], Guoliang Liu[a]*, Shengli Chen[a], Xinlin Hong[a]* and Shik Chi Edman Tsang[b]

[a] *College of Chemistry and Molecular Sciences, Wuhan University, Wuhan 430072, P R China.*

[b] *Wolfson Catalysis Centre, Department of Chemistry, University of Oxford, Oxford, OX1 3QR, UK.*

* Corresponding authors:

Email address: hongxl@whu.edu.cn; liugl@whu.edu.cn

Index

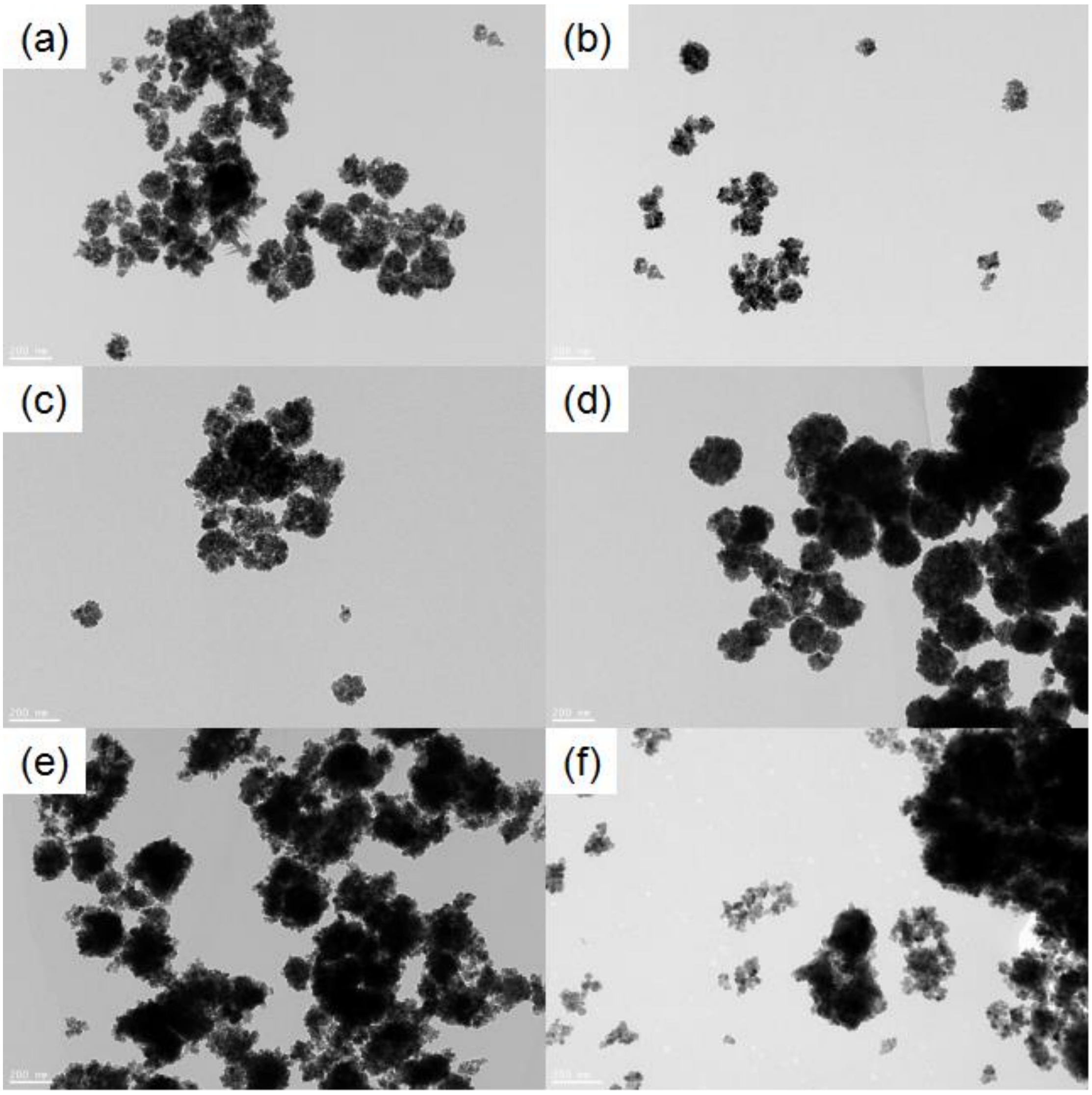

Fig. S1 TEM images of (a) CZ, (b) Pd-CZ-0.005, (c) Pd-CZ-0.01, (d) Pd-CZ-0.02, (e) Pd-CZ-0.03 and (f) Pd-CZ-0.04. All samples show the same blackberry-shaped microstructures which are composed of ZnO particles.

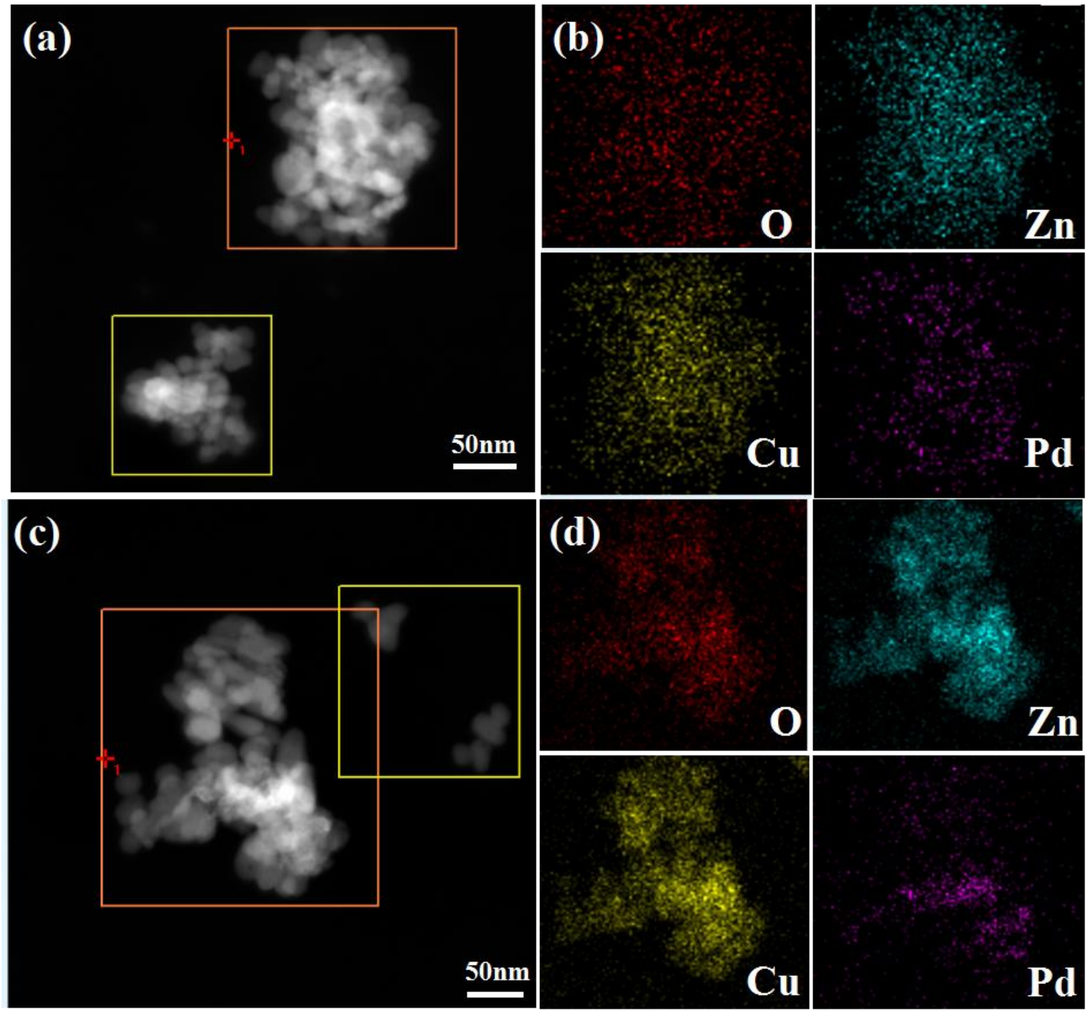

Fig. S2 HAADF-STEM images and the corresponding elemental mapping of (a, b) Pd-CZ-0.03 and (c, d) Pd-CZ-0.04. The orange rectangle is the area for STEM mapping and the yellow rectangle is for drift correction.

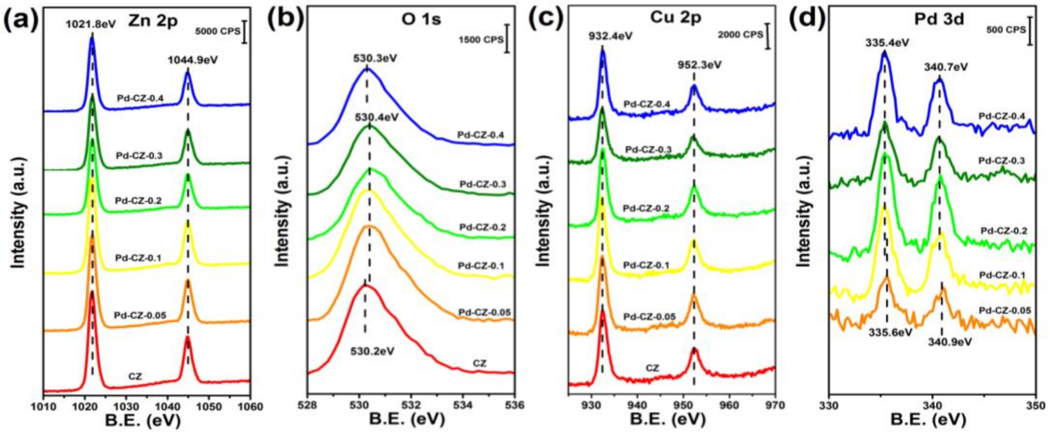

Fig. S3 XPS spectra of (a) Zn 2p, (b) O 1s, (c) Cu 2p and (d) Pd 3d for the CZ and the Pd-CZ-x samples. The binding energy values of Zn 2p, Cu 2p and Pd 3d are nearly identical for all the samples. A discernible peak shift is observed for O 1s as displayed in (b). After Pd was introduced into Cu-ZnO, O 1s BE has a positive shift of 0.1-0.2 eV, which was speculated as a result of extra Pd$^{\delta+}$-O-Zn interfaces apart from the Cu$^{\delta+}$-O-Zn interfaces in CZ as reported by Klier [1].

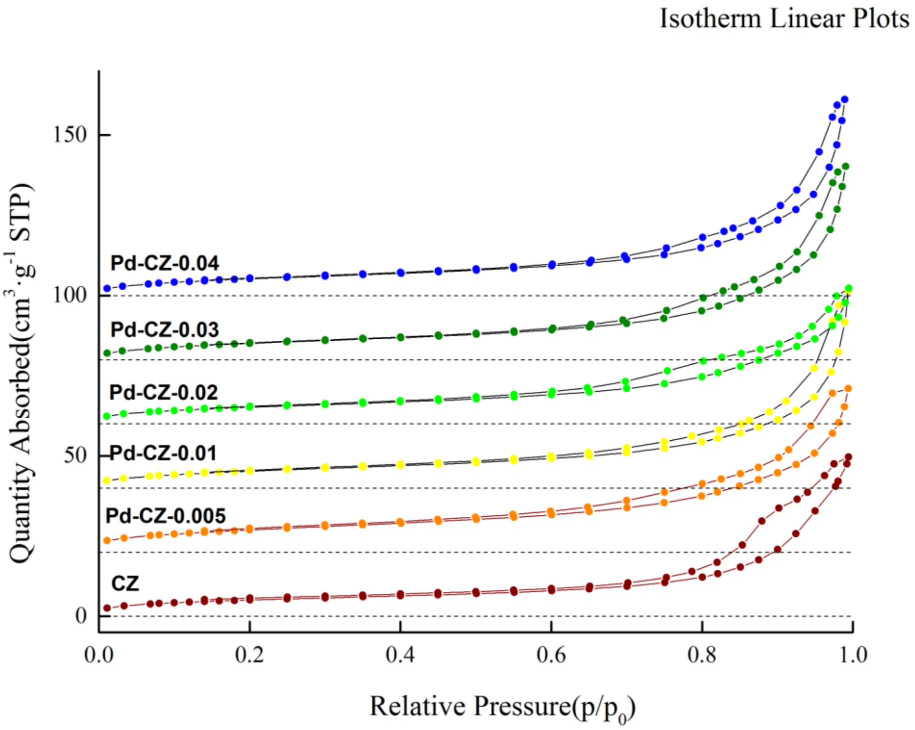

Fig. S4 N_2 sorption isotherms of different samples. All samples show a type IV pattern with a type H3 hysteresis loop, which indicates the presence of mesopores formed by the stacking of particles in the materials.

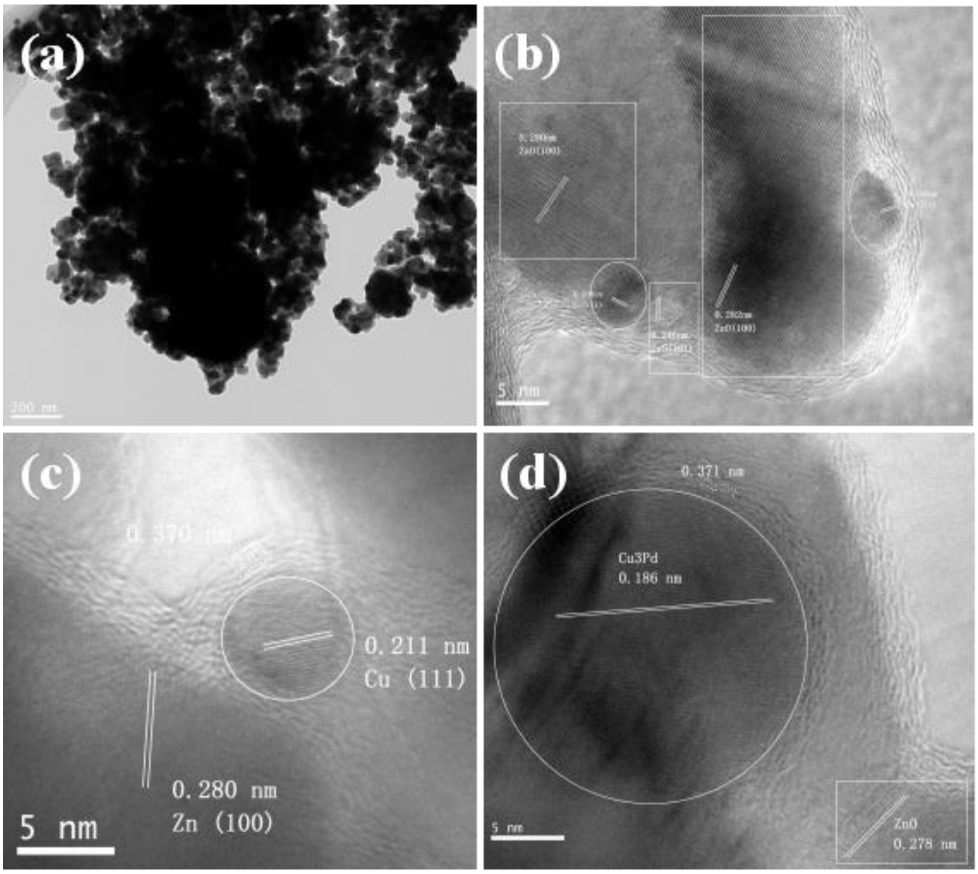

Fig. S5 TEM and HRTEM images of the used Pd-CZ-0.01 catalyst after a TOS test of 96 h. The general microstructures remain unchanged, as shown in (a). The HR-TEM images (b-d) show expanded Cu lattice fringes which were assigned to CuPd or Cu_3Pd according to the theoretical *d*-spacing values. We also find a thin shell with a distance of about 0.37 nm (c-d) was pandemic surrounding the Cu or PdCu surface, which is characteristic of amorphous ZnO as reported in reference [2].

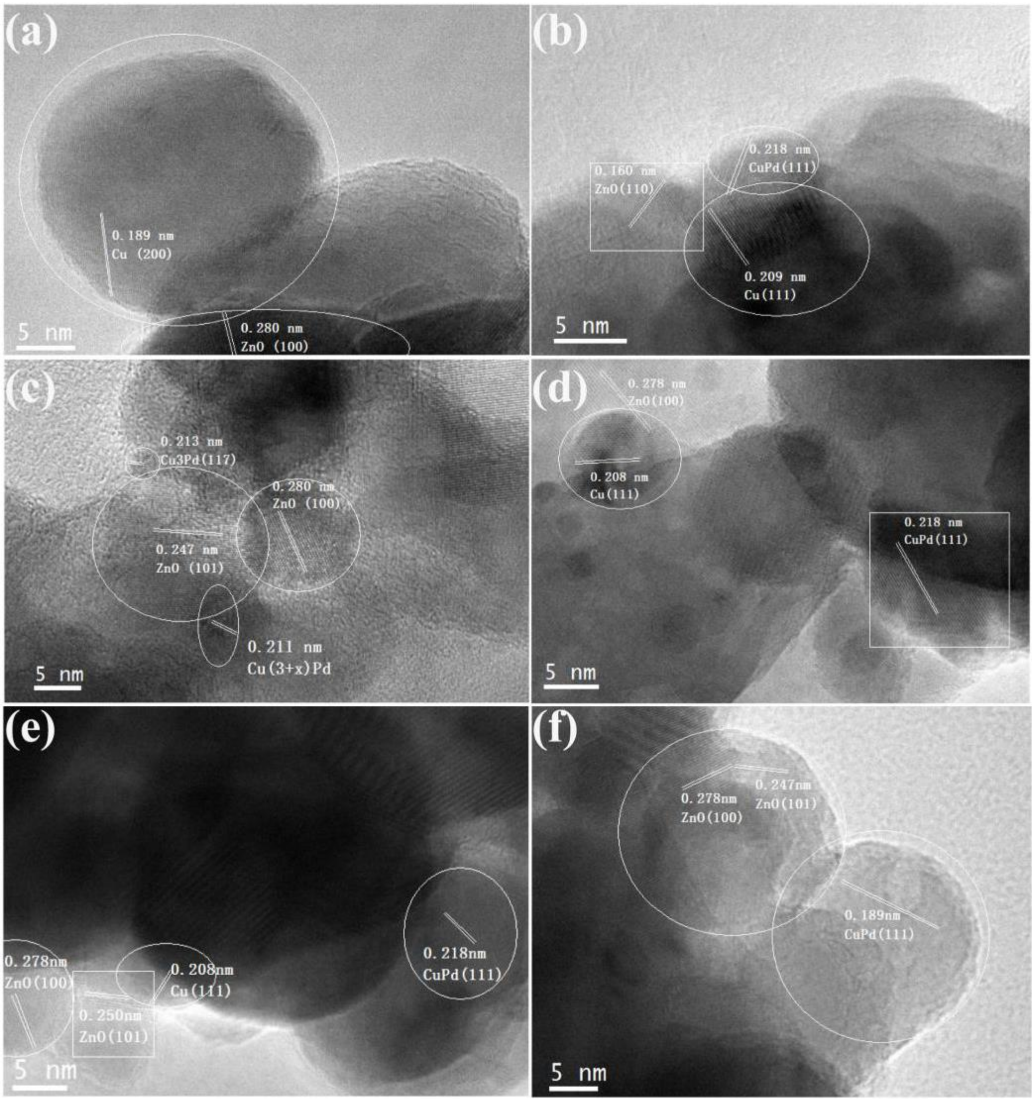

Fig.S6. HRTEM images of (a) CZ, (b) Pd-CZ-0.005, (c) Pd-CZ-0.01, (d) Pd-CZ-0.02, (e) Pd-CZ-0.03 and (f) Pd-CZ-0.04 after 8 h of catalytic tests at 513 K and 4.5 MPa. Note that each sample was cooled down in H_2 flow to room temperature after catalytic test and collected into a glass vial with a rubber cap, which was then vacuumed and N_2-refilled for several times.

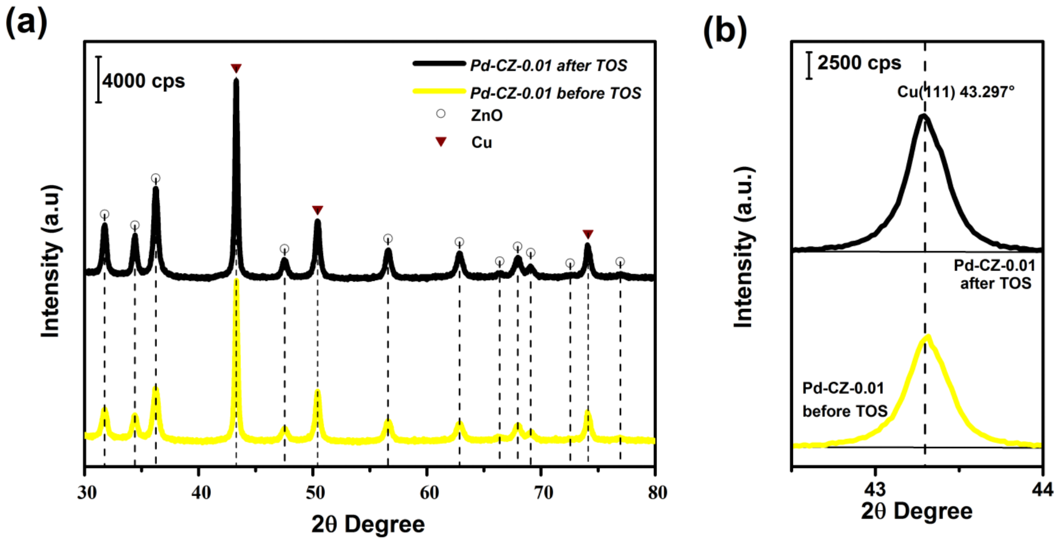

Fig. S7 PXRD patterns of Pd-CZ-0.01 before and after catalytic TOS evaluation. Through the comparison of the overall pattern in (a) and the manigified Cu (111) peak region in (b), we can find that the crystal phases in the catalyst remains unchanged.

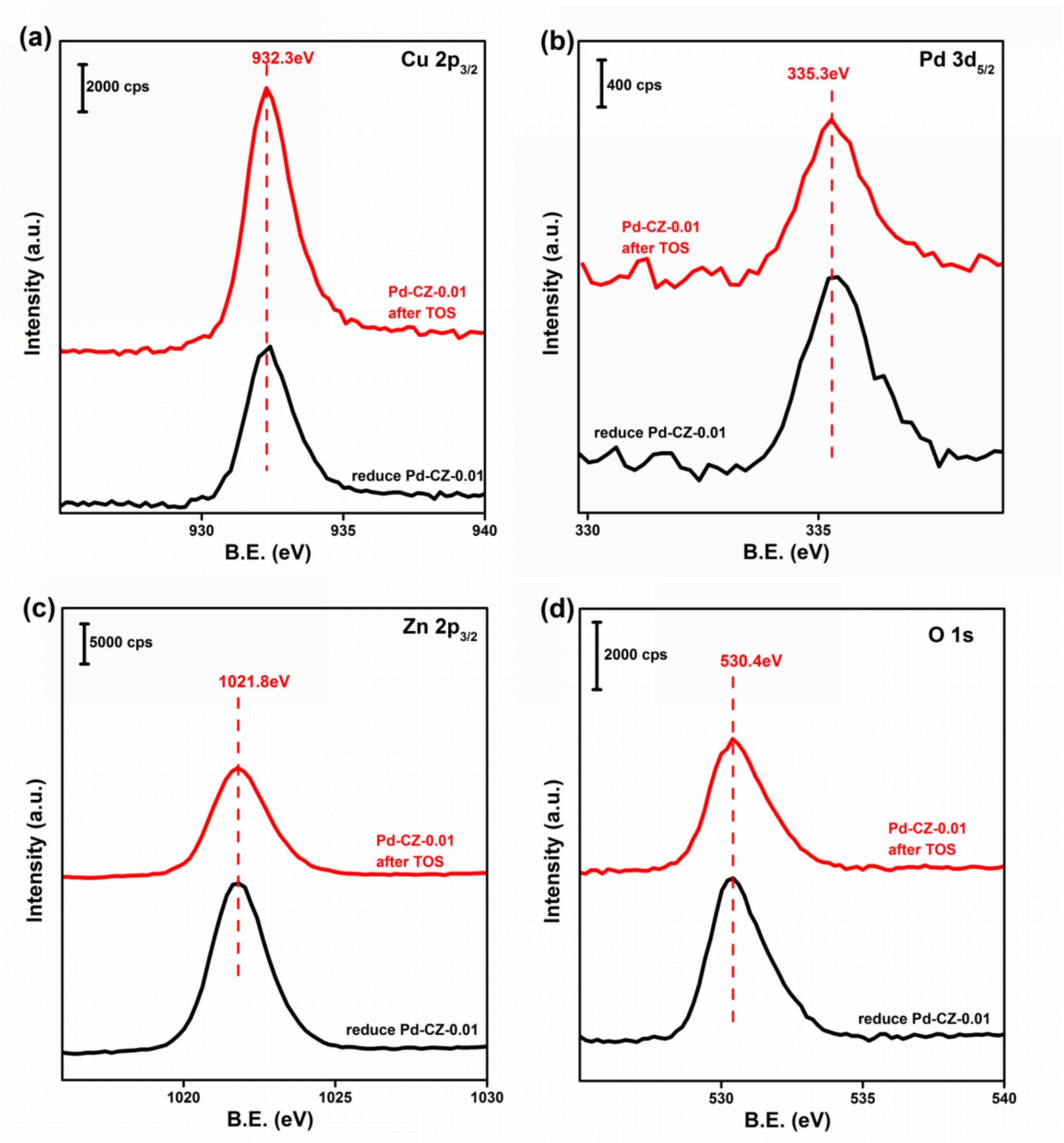

Fig. S8 A comparison of XPS spectra of four elements for Pd-CZ-0.01 before and after the TOS test. Clearly, the chemical states of all elements remain unchanged.

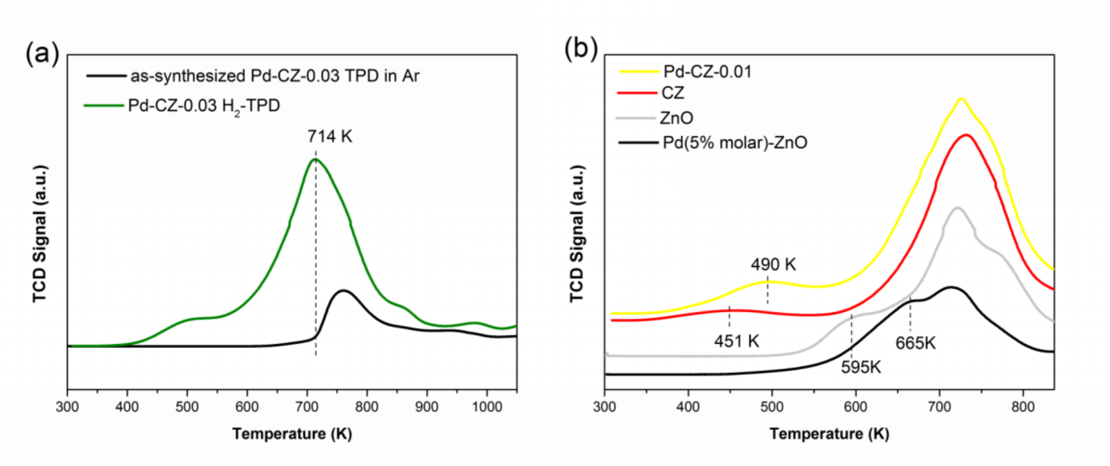

Fig. S9 (a) H_2-TPD profile (olive) and the referenced Ar-TPD profile (black) of 0.1 g of Pd-CZ-0.03. Guided by the dashed line at 714 K, it can be seen that only after the major H_2 desorption climax does the decomposition of surface carbonaceous species cause minor interference to TCD signals. (b) Other than the H_2-TPD curves of CZ and Pd-CZ-0.01 presented respectively in red and yellow lines, H_2-TPD curves of 53.3 mg of blackberry-shaped ZnO and 50 mg of Pd (5% molar)-ZnO are demonstrated in grey and black. The shoulder peaks are marked by the dashed lines.

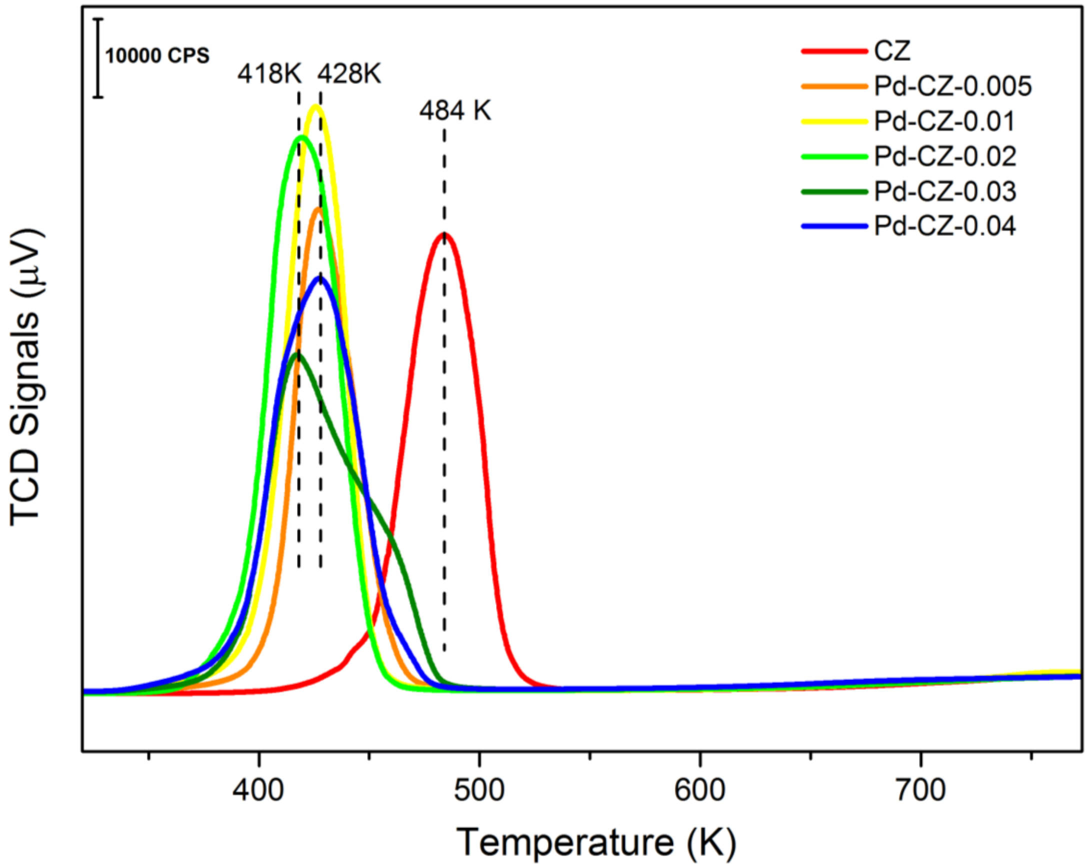

Fig.S10 TPR profiles of the pre-oxidation CZ and Pd-CZ-x catalysts. TPR conditions: 10 K min^{-1} to 773 K at a rate of 10 K min^{-1} in 30 mL min^{-1} of 5% H2/Ar. The pretreatment procedures are as follows: a) 30 mg of catayst was loaded in the quartz tube; b) Under 30 mL min^{-1} of 5% O2/He, the sample temperature was escalated at a rate of 5 K min^{-1} to 573 K and hold for 30 min; c) The gas flow was switched to 20 mL min^{-1} of Ar to let the sample cool down to ambient temperature.

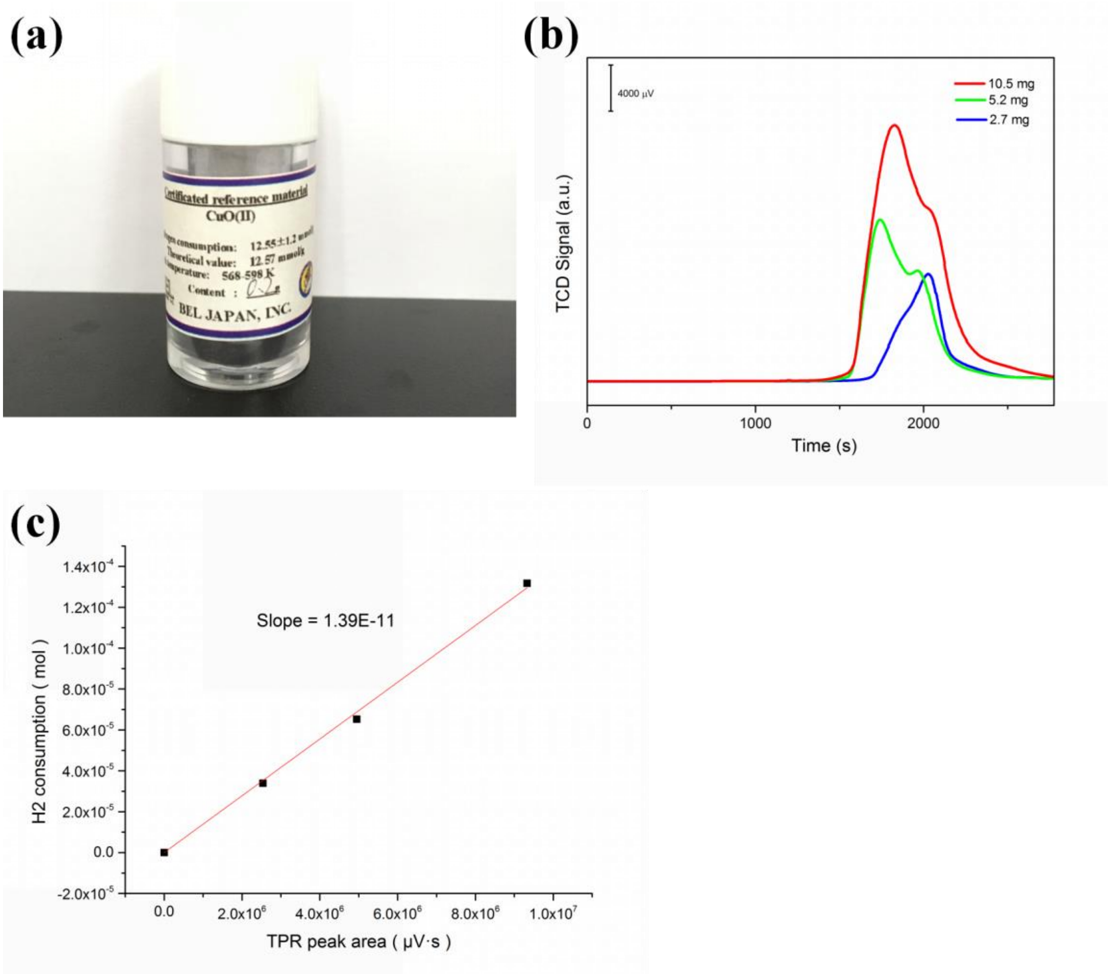

Fig. S11 (a) The CuO standard (BELCAT Co.) was used to calibrate the H_2 consumption in TPR experiments. (b) The TPR curves of three sets of TPR with different loading of standard CuO. The peak shape is deformed for the set with 2.7 mg as a result of a high proportion of powder sticking to the upper part of quartz tube far away from the furnace center. (c) The calibration plot of H_2 consumption against TPR peak area. With a combined experiment of N_2O reactive frontal chromatography (N_2O-RFC) and H_2-TPD, it has been reported that Zn can be reduced to form Cu-Zn alloy under severe reduction conditions [3]. In a more detailed and systematic work by Jehested et al., it has been verified that under 50 mbar H_2 and 493 K no metallic Zn has been observed to evolve during reduction [4]. Thus, the reduction peaks in this work can be ascribed to the reduction of surface Cu_2O alone.

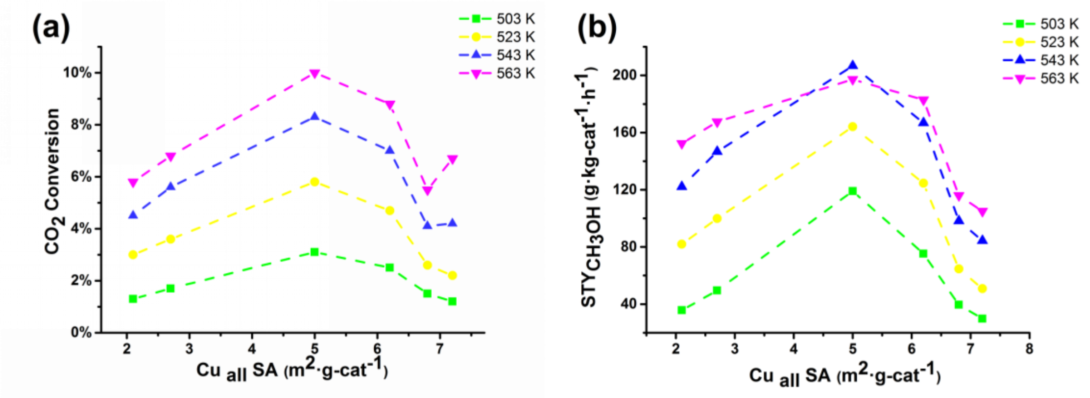

Fig. S12 Plots of (a) CO_2 conversion and (b) methanol STY against the overall Cu surface area (Cu_{all} SA).

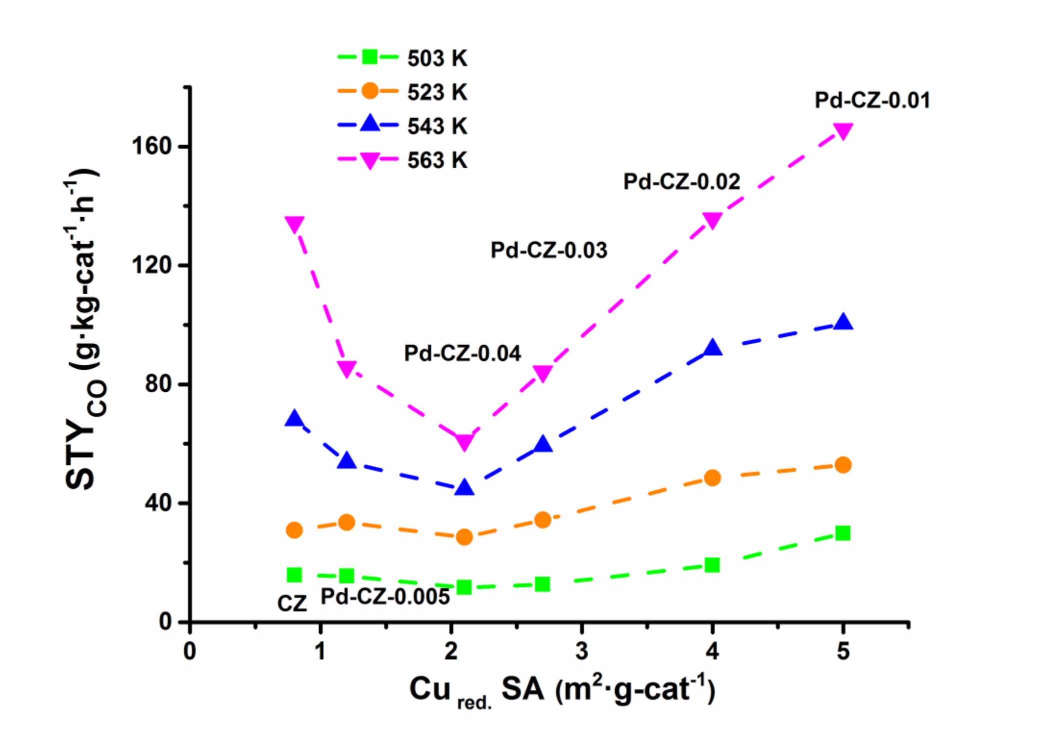

Fig. S13 The plots of CO STY against the surface area of more reducible surface Cu ($Cu_{red.}$ SA).

Table S1 The modified Auger parameters of Zn and Cu for different catalysts.

Catalyst	AP[a](Zn)	AP(Cu)
CZ	2009.55	1850.80
Pd-CZ-0.005	2009.55	1850.80
Pd-CZ-0.01	2009.60	1850.82
Pd-CZ-0.02	2009.40	1850.65
Pd-CZ-0.03	2009.40	1851.00
Pd-CZ-0.04	2009.61	1850.70
Zn[b] (II) in ZnO	2010.00 ± 0.5eV	-
Cu[b] (0)	-	1851.20 ± 0.3eV

[a] AP = BE (Zn $2p_{3/2}$ or Cu $2p_{3/2}$) - BE (Zn_{LMM} or Cu_{LMM})+ X-ray Energy. Al Kα Energy = 1486.6 eV.

[b] Refered to the values from Ref. [5].

Table S2 Crystalline size of Cu and ZnO for different catalysts.

Catalyst	Cu size (nm)[a]	ZnO size (nm)[a]
CZ	37.9	16.9
Pd-CZ-0.005	35.4	15.7
Pd-CZ-0.01	28.1	16.5
Pd-CZ-0.02	29.1	17.0
Pd-CZ-0.03	30.6	17.1
Pd-CZ-0.04	22.0	16.8

[a] The full width at half maximum (FWHM) of Cu (111) peak and ZnO (101) peak are used in size calculation by Scherrer equation.

Table S3 Active metal contents and physicochemical properties of different catalysts.

Catalysts	Active Metal Contents		BET surface area (m^2/g)	Pore volume (cm^3/g)
	Cu (wt. %)[a]	Pd (wt. %)[a]		
CZ	50.43 (43.85)	-	18.7	0.077
Pd-CZ-0.005	50.25 (43.69)	0.35 (0.37)	24.1	0.080
Pd-CZ-0.01	47.26 (43.53)	0.58 (0.73)	18.2	0.095
Pd-CZ-0.02	47.42 (43.21)	1.15 (1.45)	19.6	0.066
Pd-CZ-0.03	46.57 (42.90)	2.11 (2.16)	19.8	0.093
Pd-CZ-0.04	48.09 (42.60)	2.46 (2.85)	19.9	0.095

[a] Values in parentheses are theoretical metal content calculated based on precursor recipe.

The Cu content exceeds the theoretical value by 8.6% for Pd-CZ-0.03 to 15% for CZ. This may be rationalized by the fact that the reduction of copper by polyol as well as the hydrolysis of Zn^{2+} is accompanied by the generation of carboxylic species that hinders the complete hydrolysis of Zn^{2+} [6, 7]. The Pd content in the as-synthesized catalysts increases as more Na_2PdCl_4 is added but is lower than the theoretical value. Considering that $PdCl_4^{2-}$ has a high reducibility in polyol [7] and that its initial concentration is quite low in the DEG solution, it is possible that after catalyst synthesis a small part of palladium exists in the form of atomic cluster and this part was discarded with the supernatant during centrifugation and washing.

Table S4 Catalytic performance under different temperature were measured at pressure=4.5 MPa, H_2:CO_2=3:1, gas flow=36mL/min, catalyst mass=0.2 g (GHSV=10800).

		CZ	Pd-CZ-0.005	Pd-CZ-0.01	Pd-CZ-0.02	Pd-CZ-0.03	Pd-CZ-0.04
503 K	C[a](%)	1.2	1.5	3.1	2.5	1.7	1.3
	S[b](%)	62	69	78	78	77	73
	STY[c]	30	40	119	75	50	36
523 K	C(%)	2.2	2.6	5.8	4.7	3.6	3.0
	S(%)	59	63	73	69	72	72
	STY	51	65	164	125	100	82
543 K	C(%)	4.2	4.1	8.3	7.0	5.6	4.5
	S(%)	52	62	64	61	68	71
	STY	84	98	207	167	147	122
563 K	C(%)	6.7	5.5	10.0	8.8	6.8	5.8
	S(%)	41	54	51	54	64	69
	STY	105	116	197	183	168	152

[a] C stands for CO_2 Conversion.

[b] S stands for methanol selectivity.

[c] STY stands for methanol space-time yield in the unit of $g_{methanol}\cdot kg_{catalyst}^{-1}\cdot h^{-1}$.

References

[1] K. Klier, Adv. Catal. 31 (1982) 243-313.

[2] T. Lunkenbein, J. Schumann, M. Behrens, R. Schloegl, M.G. Willinger, Angew. Chem. Int. Ed. 54 (2015) 4544-4548.

[3] H. Wilmer, O. Hinrichsen, Catal. Lett. 82 (2002) 117-122.

[4] S. Kuld, C. Conradsen, P.G. Moses, I. Chorkendorff, J. Sehested, Angew. Chem. Int. Ed. 53 (2014) 5941-5945.

[5] P. Swift, D. Shuttleworth, M.P. Shea (Eds.), Practical Surface Analysis by Auger and X-ray Photoelectron Spectroscopy, Wiley, London, 1983, p. 477.

[6] B.W. Chieng, Y.Y. Loo, Mater. Lett. 73 (2012) 78-82.

[7] Y.J. Xiong, J.Y. Chen, B. Wiley, Y.N. Xia, S. Aloni, Y.D. Yin, J. Am. Chem. Soc. 127 (2005) 7332-7333.

[8] F. Arena, G. Mezzatesta, G. Zafarana, G. Trunfio, F. Frusteri, L. Spadaro, J. Catal. 300 (2013) 141-151.